

CFD evaluation of mean pollutant concentration variations in step-down street canyons

Nicolas Reiminger^{1,2*}, José Vazquez², Nadège Blond³, Matthieu Dufresne¹, Jonathan Wertel¹

¹AIR&D, 67400, Illkirch-Graffenstaden, France

²ICUBE Laboratory, CNRS/University of Strasbourg, 67000, Strasbourg, France

³LIVE Laboratory, CNRS/University of Strasbourg, 67000, Strasbourg, France

*Corresponding author: Tel. +33 (0)3 69 06 49 40, Mail. nreiminger@air-d.fr

Citation : Reiminger, N., Vazquez, J., Blond, N., Dufresne, M., & Wertel, J. (2020). CFD evaluation of mean pollutant concentration variations in step-down street canyons. *Journal of Wind Engineering and Industrial Aerodynamics*, 196, 104032. <https://doi.org/10.1016/j.jweia.2019.104032>

Abstract:

Atmospheric pollution became a big issue in densified urban areas where the ventilation in streets is not sufficient. It is particularly the case for street surrounded by high buildings so-called street canyons. The ventilation and, thus, the concentrations in this kind of street are highly relying on geometric properties of the street (width of the street, heights of the buildings, etc.). Reynolds-averaged Navier-Stokes equations are used to investigate the impact of two geometric street ratios on pollutant dispersion: the ratio of the leeward to the windward building height ($H1/H2$) and the ratio of the street width to the windward building height ($W/H2$). The aim is to quantitatively assess the evolution of mean pollutant concentrations in the case of step-down street canyons with $H1/H2$ ranging from 1.0 to 2.0 and street width ratios $W/H2$ ranging from 0.6 to 1.4. Three types of recirculation regimes could be established, depending on the number and the direction of the vortices occurring inside and outside the canyon. Evolution of pollutant concentrations as a function of both ratios is provided as well as the recommended regimes in the perspective of reducing pollutant concentration in step-down street canyons at pedestrian level and near building faces.

Keywords: Air quality, Computational fluid dynamics, Street Canyon, Aspect ratio, Building characteristics

Highlights

- Standard and RNG k- ϵ models give almost the same critical values $H1/H2$
- Three types of regimes may occur in the canyon for $0.6 < W/H2 < 1.4$ and $1.0 < H1/H2 < 2.0$
- Concentrations do not depend on the building height ratio in the case of regime A
- Regime A is the best for mitigating atmospheric pollution in street canyons
- Regime C occurs for high $H1/H2$ and low $W/H2$, giving very high mean concentrations

1. Introduction

Air quality has become a major concern, especially in urban areas where air pollutant sources are numerous and population density is high. Air quality is influenced by traffic-related emissions and the local atmospheric environment which is highly dependent on street geometry. Indeed, narrow streets surrounded by high buildings are more often subject to high pollutant concentrations than wide streets with lower building heights, due to poorer ventilation. An estimation of pollutant concentrations in streets depending on building configurations could help urban planners to understand the impacts of street geometry on air quality and provide keys to making suitable choices to lessening air pollution levels, as one of the key point discussed by Bibri and Krogstie (2017) in order to achieve smart sustainable cities of the future.

The effects of street geometry on pollutant dispersion have already been studied extensively with both experimental (Gerdes and Olivari, 1999; Hotchkiss and Harlow, 1973; Pavageau and Schatzmann, 1999; Vardoulakis et al., 2003) and numerical methods (Aristodemou et al., 2018; Bijad et al., 2016; Santiago and Martin, 2005; Tominaga and Stathopoulos, 2017; Vardoulakis et al., 2003) and also at full-scale with in situ measurements (Qin and Kot, 1993; Vardoulakis et al., 2002). Some authors have even studied the effects of roof shape on pollutant dispersion (Takano and Moonen, 2013; Wen and Malki-Epshtein, 2018). However, most of these works were conducted in symmetrical street canyons using buildings with the same height. Indeed, streets surrounded by buildings of the same height do exist although streets with different building heights, so-called asymmetrical street canyons, are found more often. Addepalli and Pardyjak (2015) studied cases of step-down street canyons with a taller building on the leeward side and showed that there are significant modifications of flow patterns depending on building height and street width ratios. Xiaomin et al. (2006) performed a similar work with different kinds of streets, including deep and wide symmetrical streets and step-up and step-down asymmetrical streets, and showed that there are three major types of regimes in street canyons depending on height and width ratios, especially in the case of step-down street canyons. In spite of the several studies already done, and although there is a need for urban planners and decision makers, quantitative information on how concentrations evolve with the modification of street geometry is still lacking. Thus, further work is required in this direction.

The aim of this work is to provide information on how mean pollutant concentrations quantitatively evolve in a step-down street canyons. More specifically, it is to assess the evolution of concentration in the street according to two specific ratios: the ratio of the leeward building height to the windward building height ($H1/H2$), and the ratio of the street width to the windward building height ($W/H2$). This assessment is carried out using computational fluid dynamics (CFD) simulations. Section 2 presents the numerical model used in this work with the governing equations, the boundary conditions and the numerical settings. Section 3 presents the validation of the model versus experimental data in which a mesh sensitivity test and an evaluation of the best turbulent Schmidt number are carried out. Finally, section 4 describes the results of the study for several mean concentrations and a discussion of the results is proposed in section 5.

2. Numerical model

2.1. Computational domain and boundary conditions

Fig. 1 shows the computational domain of the street canyon, the dimensions of interest, the localization of the different boundary conditions and the emission source as well as the domain size.

In this study, H_1 corresponds to the height of the leeward building, H_2 corresponds to the height of the windward building, W corresponds to the width between the two buildings and L corresponds to the length of the street. Here, we study the case of long canyons ($L/W > 7$) (Vardoulakis et al., 2003) with the assumption that the interactions in the y -direction are negligible. To ensure this assumption a 3D simulation was computed for this study, and the results were compared to 2D results. Using a street canyon with $L/W = 10$, it was found that the differences between 2D and 3D simulation are fewer than 8% for $|y| \leq 3H$ with $y = 0H$ the center plane of the street. For $3H < L/W < 5H$, differences are still acceptable but can reach 20% (more details can be found in the appendix 1). According to this results, all simulations were done in 2D in order to reduce calculation costs.

We followed the recommendations given by Franke et al. (2007) concerning the boundary conditions and the domain size: the inlet boundary is placed $7 \times H_2$ away from the canyon; a symmetry condition is applied at the top and the lateral boundaries, with the top placed $6 \times H_2$ away from the roofs of the buildings; the outlet boundary is placed $15 \times H_2$ away from the street to allow for flow development using a freestream outlet, and no-slip conditions were applied to all the other boundaries (roofs/walls of the buildings and the ground).

Lastly, traffic exhaust is modelled by a line source along the middle of the street ($x=0$) where a source term of emission is added in the pollutant transport equation. The source term corresponds to a mass flow rate chosen to $1.10^{-4} \mu\text{g/s}$.

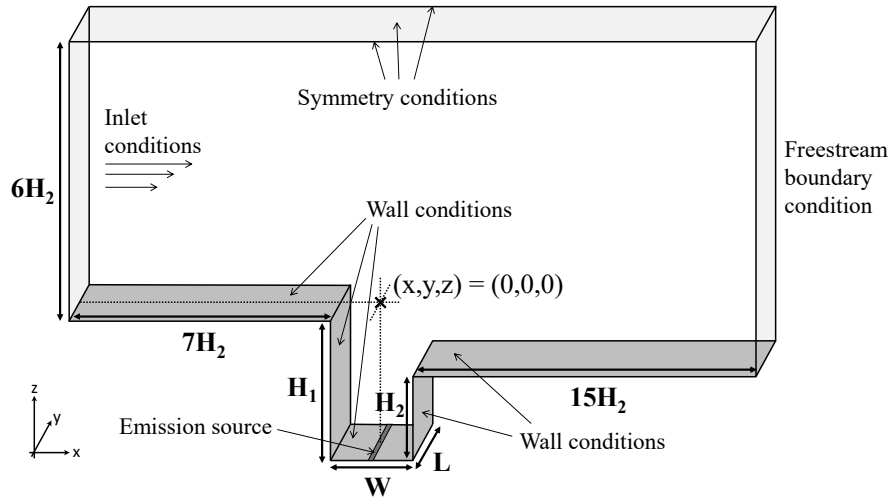


Fig. 1. Sketch of the computational domain

2.2. Governing equations

CFD simulations were carried out in OpenFOAM 5.0. Since in real contexts, full steady state is not always reached, all the simulations were performed using the unsteady pimpleFoam solver which is able to capture time instabilities. Reynolds-averaged Navier-Stokes (RANS) methodology was used to solve the continuity and the momentum equations throughout the computational domain by considering air as an incompressible fluid. This assumption can be made because of the low wind velocities ($< 5\text{m/s}$) giving Mach numbers under 0.3 (Anderson, 2009). The corresponding continuity (1) and momentum (2) equations are given below:

$$\frac{\partial \bar{u}_i}{\partial x_i} = 0 \quad (1)$$

$$\frac{\partial \bar{u}_i}{\partial t} + \frac{\partial (\bar{u}_i \bar{u}_j)}{\partial x_j} = -\frac{1}{\rho} \left(\frac{\partial \bar{P}}{\partial x_i} \right) + \nu \left(\frac{\partial^2 \bar{u}_i}{\partial x_j \partial x_j} \right) - \frac{\partial \overline{u'_i u'_j}}{\partial x_j} \quad (2)$$

where \bar{u}_i and u'_i are the i th mean and the fluctuating velocities, respectively, x_i is the i th Cartesian coordinate, \bar{P} is the mean pressure and ν is the kinematic viscosity.

Using RANS to solve turbulent flows requires choosing a turbulence model to solve the Reynolds stress tensor $\overline{u'_i u'_j}$ (3). The RNG k- ϵ turbulence model proposed by Yakhot et al. (1992) was chosen for turbulent closure because the numerical results fitted well with the experimental data (see section 3.1.). The corresponding equations for turbulent kinetic energy (4) and turbulent dissipation rate (5) of the RNG model are given below. Taking $R=0$ and using the correct constants, these equations also correspond to the standard k- ϵ turbulence model.

$$\overline{u'_i u'_j} = \frac{2}{3} k \delta_{ij} - \nu_t \left(\frac{\partial \bar{u}_i}{\partial x_j} + \frac{\partial \bar{u}_j}{\partial x_i} \right) \quad (3)$$

$$\frac{\partial k}{\partial t} + \bar{u}_j \frac{\partial k}{\partial x_j} = \frac{\partial}{\partial x_j} \left(\frac{\nu_t}{\sigma_k} \frac{\partial k}{\partial x_j} \right) + \nu_t \left(\frac{\partial \bar{u}_i}{\partial x_j} + \frac{\partial \bar{u}_j}{\partial x_i} \right) \frac{\partial \bar{u}_i}{\partial x_j} - \epsilon \quad (4)$$

$$\frac{\partial \epsilon}{\partial t} + \bar{u}_j \frac{\partial \epsilon}{\partial x_j} = \frac{\partial}{\partial x_j} \left(\frac{\nu_t}{\sigma_\epsilon} \frac{\partial \epsilon}{\partial x_j} \right) + \frac{\epsilon}{k} \left(C_{\epsilon 1} \nu_t \left(\frac{\partial \bar{u}_i}{\partial x_j} + \frac{\partial \bar{u}_j}{\partial x_i} \right) \frac{\partial \bar{u}_i}{\partial x_j} - C_{\epsilon 2} \epsilon \right) - R \quad (5)$$

$$R = \frac{C_\mu \eta^3 (1 - \eta / \eta_0) \epsilon^2}{1 + \beta \eta^3} \frac{\epsilon^2}{k} \quad (6)$$

$$\nu_t = C_\mu \frac{k^2}{\epsilon} \quad (7)$$

where $\eta = Sk/\epsilon$ and $S^2 = 2S_{ij}S_{ij}$ the mean strain tensor, \bar{u}_i is the i th mean velocity, x_i is the i th Cartesian coordinate, ν is the kinematic viscosity, k is the turbulent kinetic energy, ϵ is the turbulent dissipation rate, δ_{ij} is the Kronecker delta and ν_t is the turbulent viscosity. All the other parameters are model constants given in Table 1 for both the standard and the RNG k- ϵ turbulence models.

Table 1. Turbulence model constant values

Model	C_μ	$C_{\epsilon 1}$	$C_{\epsilon 2}$	σ_k	σ_ϵ	η_0	β
Standard k- ϵ	0.09	1.45	1.9	1.0	1.3	-	-
RNG k- ϵ	0.085	1.42	1.68	0.72	0.72	4.38	0.015

Pollutants are considered as passive scalars since no chemical effects are solved in this study. The equation governing advection-diffusion for the passive pollutant dispersion given in OpenFOAM was modified to take into account turbulent diffusivity. The corresponding equation is given below:

$$\frac{\partial C}{\partial t} + \frac{\partial (u_i C)}{\partial x_i} - \frac{\partial}{\partial x_i} \left[\left(D_m + \frac{\nu_t}{Sc_t} \right) \frac{\partial C}{\partial x_i} \right] = E \quad (8)$$

where C is the pollutant concentration, D_m is the molecular diffusion coefficient, Sc_t is the turbulent Schmidt number and E is the source term of the pollutants (emissions).

The ratio ν_t/Sc_t corresponds to the turbulent diffusion coefficient. The value of Sc_t is constant throughout the computational domain and fixed at 0.2. This value was chosen for the validation step (see section 3.2.).

2.3. Numerical settings

Second order schemes were adopted for all the gradient, divergent and Laplacian terms. In particular, for the Laplacian terms we used the ‘Gauss linear corrected’-scheme which is an unbounded second order conservative scheme, the second order ‘Gauss linear’-scheme for the gradient terms and the ‘Gauss linearUpwind’-scheme for the divergent terms, the latter scheme being an unbounded upwind second order scheme.

All the simulations were run until the convergence was reached. To ensure the convergence of the simulations, the values of the streamwise velocity U and the pollutant concentration C were monitored for several points all over the canyon. Since all the simulations reached steady-state, they were stopped when the values monitored were constant over time. Moreover, at the end of the simulations all the residuals were under 10^{-5} .

3. Model validation

The model was validated versus the experimental wind tunnel data proposed by Soulhac et al. (2001). This experiment consists of a regular street canyon with $H1/H2=1$ and $W/H2=1$ with a gas released continuously at the center of the street. A summary of the boundary conditions used for this validation is given in Table 2. A comparison between experimental and numerical streamwise velocity was made to evaluate mesh sensitivity; another comparison between experimental and numerical pollutant concentrations was made to find the turbulent Schmidt number which gave the best results compared to the experiment.

Table 2. Summary of the boundary conditions

Inlet	<p>Experimental velocity profile which corresponds to a power law profile with $U = U_{ref} \left(\frac{z}{z_{ref}} \right)^\alpha$, where $U_{ref}=5.54\text{m/s}$ is the velocity at z_{ref}, $z_{ref}=0.63\text{m}$ is the reference height, $\alpha=0.127$ is the power law exponent and z the height from the ground.</p> <p>$k = 1.5(UI)^2$, with $I \approx 0,16.Re^{-1/8}$ the turbulent intensity, with $Re = U.H/\nu$ the Reynolds number where $U=4.43\text{m/s}$ is the mean inlet velocity, $H=0.6\text{m}$ is the injection height and $\nu=1.56.10^{-5}$ is the kinematic viscosity.</p> <p>$\epsilon = C_\mu^{0,75} \frac{k^{1,5}}{l}$ with $C_\mu=0.085$ the CFD constant, and l the turbulence length taken as equal to the injection height (0.6m).</p> <p>The inlet profiles start from the upwind roof height ($z=0$) and end at the domain top height ($z=6H_2$).</p>
Outlet	Freestream outlet
Top	Symmetry plane
Lateral surfaces	Symmetry plane
Ground and building surfaces	No slip condition ($U=0\text{m/s}$)
Emission	Line source with emission rate $q_m=1.10^{-4} \mu\text{g/s}$ localized at the middle of the street

3.1. Mesh sensitivity

Mesh sensitivity tests were carried out and compared to the experimental streamwise velocity results to find the best compromise between the precision of the numerical results and calculation costs.

Fig. 2 shows this comparison for three localized velocity profiles: on the leeward side of the street ($x/H=-0.2$), in the middle of the street ($x/H=0.0$) and on the windward side of the street ($x/H=0.2$). Three mesh-dependent results are proposed and the grid expansion ratio between the coarse and the medium grid and between the medium and the fine grid is 2. Velocities and heights are proposed in dimensionless form, corresponding to U/U_{max} with $U_{max}=5\text{m/s}$ and z/H with $H=0.1\text{m}$, respectively.

The results show good agreement between the experimental and numerical data whatever the mesh refinement considered. There is a noticeable difference in the numerical results between the coarse and the medium mesh in the street canyon ($z/H < 1$). The difference between the medium and the fine meshes is almost imperceptible apart from the low heights for which the fine mesh results are closer to the experimental results. Thus, in the light of these results, the fine mesh grid was adopted, and an illustration of the selected meshing is provided in Fig. 3.

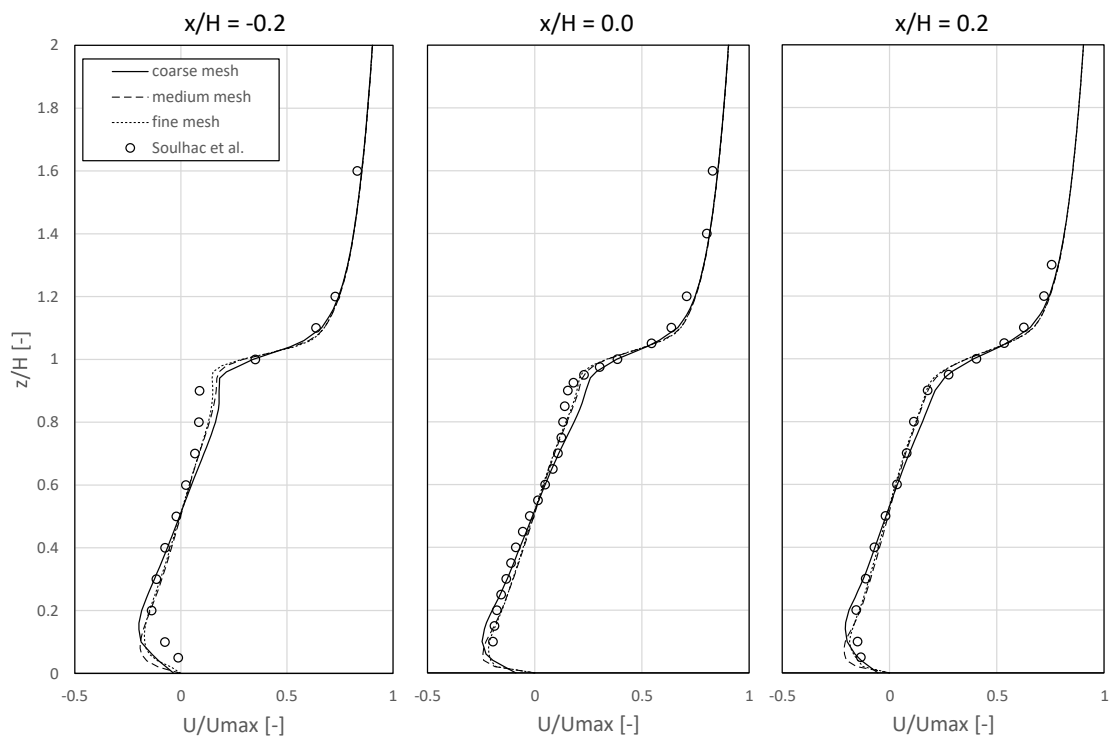


Fig. 2. Vertical distribution of numerical streamwise velocities for different mesh refinements compared to Soulhac et al. (2001) experimental data

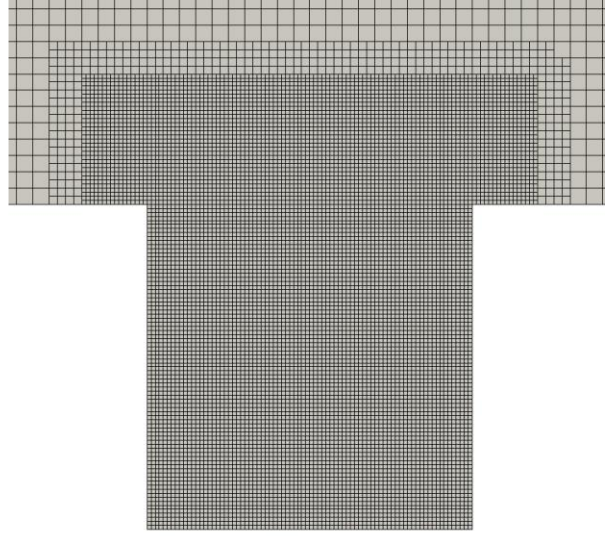


Fig. 3. Illustration of the selected meshes

An additional mesh sensitivity study was performed on the variable of interest C , the pollutant concentration, using the Grid Convergence Index (GCI) methodology proposed by Roache (1994). This methodology is used to assess the mesh-related errors of a given mesh grid in view of the fine and coarse grid results and depending on the grid expansion ratio and the order of the numerical scheme used. The GCI for fine mesh grid error evaluation is given below:

$$GCI_{fine\ grid} = 3 \frac{|f_2 - f_1|}{f_1} (r^p - 1)^{-1} \quad (9)$$

where f_1 and f_2 are the results using the fine and coarse grid, respectively (here $f_1 = C_{fine}$ and $f_2 = C_{coarse}$), r is the grid expansion ratio between the fine and the coarse grid and p is the order of the numerical scheme.

The grid convergence index for the fine grid was calculated for 370 points uniformly distributed in the street canyon with $p = 2$ (second order schemes) and $r = 4$ (the fine mesh is four times smaller than the coarse mesh). The corresponding mean $GCI_{fine\ grid}$ is 2% and the maximum 4%, thus corresponding to a sufficient grid resolution. The typical dimension of the chosen cells is $0.0125 \times H_2$.

3.2. Turbulent Schmidt number

According to Tominaga and Stathopoulos (2007), the optimal values of the turbulent Schmidt number Sc_t are widely spread between 0.2 and 1.3 and have a considerable influence on pollutant mass transfer. Thus, Sc_t must be chosen with care. To make this choice, several simulations were performed for $0.1 < Sc_t < 0.7$ with steps of 0.1 and the results were compared with the experimental data.

Fig. 4 shows the results for three localized concentration profiles: close to the leeward building ($x/H = -0.4$), in the middle of the street ($x/H = 0.0$) and close to the windward building ($x/H = 0.4$). The three closest numerical results compared to the experiment are shown and differ only by the turbulent Schmidt number used: 0.1, 0.2 and 0.3. Concentrations and heights are proposed in dimensionless form. The same dimensionless form as before was used for the heights (z/H) and the dimensionless concentration was obtained using (10).

$$C^* = C \cdot U_H \cdot H_2 \cdot L / q_m \quad (10)$$

where C^* is the dimensionless concentration, C is the concentration, U_H is the velocity just over the windward building ($0.05H_2$ over the roof) and far from the canyon in the experimental setup of Soulhac et al. (2001) with $U_H = 2.75$ m/s, H_2 is the windward building height, L is the pollutant injection length and q_m is the pollutant emission rate.

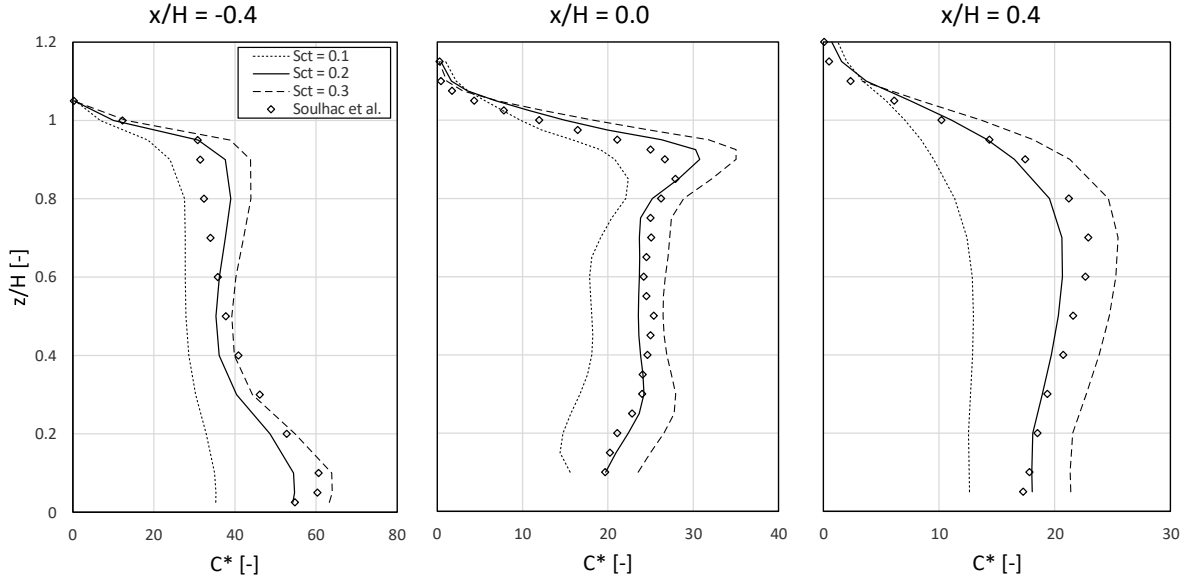


Fig. 4. Vertical distribution of numerical dimensionless concentrations for different Sc_t compared to Soulhac et al. (2001) experimental data

The results show good agreement between the numerical and experimental data for $Sc_t=0.2$. Regarding this turbulent Schmidt number, for the leeward side there is generally an overestimation of the concentrations in the upper part of the street and an underestimation in the lower part of street while there is a general underestimation for the windward side. The numerical results are less accurate with $Sc_t=0.1$ and $Sc_t=0.3$, so the value of 0.2 was kept for the rest of the study. Using this turbulent Schmidt number, the mean normalized absolute error over the experimental profiles was 10%. The corresponding 95th percentile was less than 30% and the maximal differences between the experimental and numerical results occurred near the ground.

The models used in the present paper (RANS and RNG $k-\epsilon$) give a global underestimation of the turbulent momentum diffusion leading to low turbulent Sc_t . The turbulent Schmidt number taken as 0.2 is in coherence with other authors results who took a low Sc_t as 0.3 for the same models (Tominaga and Stathopoulos, 2007). It should be noted that the value of 0.2 could not be the best for all the geometric ratios considered in this work. However, it was decided to always use the same Sc_t in the whole study, which is a common practice done by the scientific community (Takano and Moonen, 2013 ; Wen and Malki-Epshtein, 2018 ; Cui et al., 2016), in order to only compare the influence of the geometric properties of the buildings on the mean concentrations and to avoid multi parameter comparisons.

4. Effects of street dimensions on mean concentrations

Exactly the same conditions as defined previously were used for the present study, except for the geometric properties of the street and in particular H_1 and W . To study the mean concentrations in the street canyon, several couples of height ratios H_1/H_2 and width ratios W/H_2 were considered. The present work is limited to a step-down street canyon configuration where $H_1/H_2 > 1.0$. The following height ratios were used: 1.0, 1.2, 1.4, 1.6, 1.8 and 2.0. For each of these height ratios, 5 width ratios were considered: 0.6, 0.8, 1.0, 1.2 and 1.4, giving a total number of 30 simulations and an

overall idea of how could evolve mean concentrations in step-down street canyons. This number does not include certain particular cases that were also simulated when the results were strongly different between two cases (e.g. when for a given width ratio, two successive height ratios results in two different regimes). A case table of all the ratios considered in this work is proposed in Table 3.

Table 3. Case table of all geometric ratios considered (● : couples of ratios initially considered, ○ : specific cases considered aftermath)

W/H_2	H_1/H_2				
	0.6	0.8	1.0	1.2	1.4
2.0	●	●	●	●	●
1.9					
1.8	●	●	●	●	●
1.7					
1.6	●	●	●	●	●
1.5		○			
1.4	●	●	●	●	●
1.3			○	○	○
1.2	●	●	●	●	●
1.1	○	○			
1.0	●	●	●	●	●

Fig. 5 shows the localization of the mean concentrations studied in this paper. Here, we study:

- The concentration averaged all over the street (in the $W \times H_2$ area),
- The mean concentration on a vertical profile placed $0.1H_2$ from the windward building facade (concentration averaged for the H_2 height) and another vertical profile placed $0.1H_2$ from the leeward building facade (concentration averaged for the H_2 height). These mean concentrations are relevant for people living in the buildings near the street.
- The mean concentration for a horizontal profile placed $0.1H_2$ from the ground (concentration averaged for the W length). This mean concentration is relevant for pedestrians in the street.

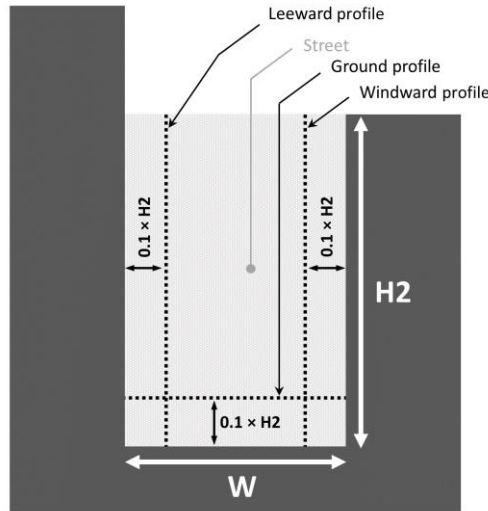


Fig. 5. Localization of the mean concentrations studied.

All the concentrations will be given in dimensionless form. The dimensioned concentrations could also be retrieved using (10) with $U_H=2.75\text{m/s}$, $H_2=0.1\text{m}$, $L=0.0025\text{m}$ and $q_m=1.10^{-4}\ \mu\text{g/s}$.

4.1. Vorticity and recirculation regimes in the street canyon

Flow velocities and recirculation patterns have a significant impact on pollutant dispersion and thus on pollutant concentrations inside and outside the street canyon. The modifications of flow velocities and recirculation patterns are caused solely by the geometric properties of the street ($H1/H2$ and $W/H2$) as all the simulations were run using the same velocity inlet profile.

Out of the total number of simulations performed, three types of recirculation regimes were found. Fig. 6 shows an example of each regime with the velocity vectors and the corresponding y -vorticity ω_y , given by equation (11). These three regimes stand out due to their number of recirculation zones inside and outside the canyon.

$$\omega_y = \frac{\partial U_x}{\partial z} - \frac{\partial U_z}{\partial x} \quad (11)$$

Regime A corresponds to a big single vortex localized in the canyon. For this regime, vorticity is globally positive in the canyon, which means that the vortex rotates clockwise. Regime B corresponds to two vortices, one large vortex in the canyon and a second localized mostly over the canyon and the windward building. The large vortex in the canyon is very similar to that of regime A, but here the vorticity is mostly negative, and the vortex rotates counterclockwise. The second vortex localized outside the canyon rotates clockwise. Regime C corresponds to three vortices, two contra-rotative vortices localized in the canyon and the third vortex mostly localized over the windward building. This regime appears to be a combination of regimes A and B, with the clockwise-vortex of regime A in the low part of the street and the counterclockwise-vortex of regime B situated just over it. The same clockwise-outside-vortex of regime B is also observed.

Xiaomin et al. (2006) gave the critical value of $H1/H2$ for several $W/H2$ corresponding to the limit between regime A and regime B/C without distinction between B and C. Their results are compared with those of the present study for $W/H2$ from 0.6 to 1.4 and are shown in Fig. 7 with the gray area corresponding to the switching area between regime A and regime B/C. The boundary conditions were the same between both studies.

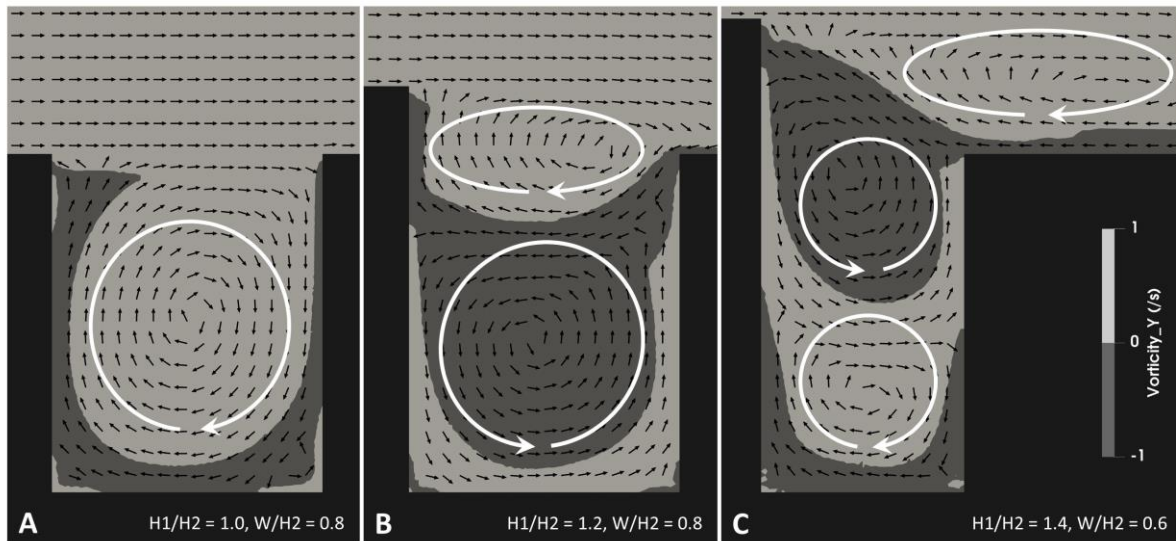


Fig. 6. Recirculation patterns, velocity vectors and y-vorticity for different geometric ratios $H1/H2$ and $W/H2$

The results obtained after the simulations showed a trend similar to that of the results of Xiaomin et al. (2006). The critical value of $H1/H2$ increases when the distance between the buildings increases and the zone of change between regime A and regime B/C is quite similar for both studies. However, critical values seem to be reached sooner according to our results (i.e. for smaller $H1/H2$) with a maximal difference of 0.1 compared to the results of Xiaomin et al. (2006).

Some simulations were rerun using the turbulent conditions of Xiaomin's et al. (2006), that is, using the standard $k-\epsilon$ turbulent closure. The results, also presented in Fig. 7, show this time perfect concordance between both studies. Thus, turbulent closure schemes have an influence on the critical values of $H1/H2$. This difference between critical values when using standard $k-\epsilon$ or RNG $k-\epsilon$ are, however, quite small with a maximum difference of 0.1 for the ratio $H1/H2$.

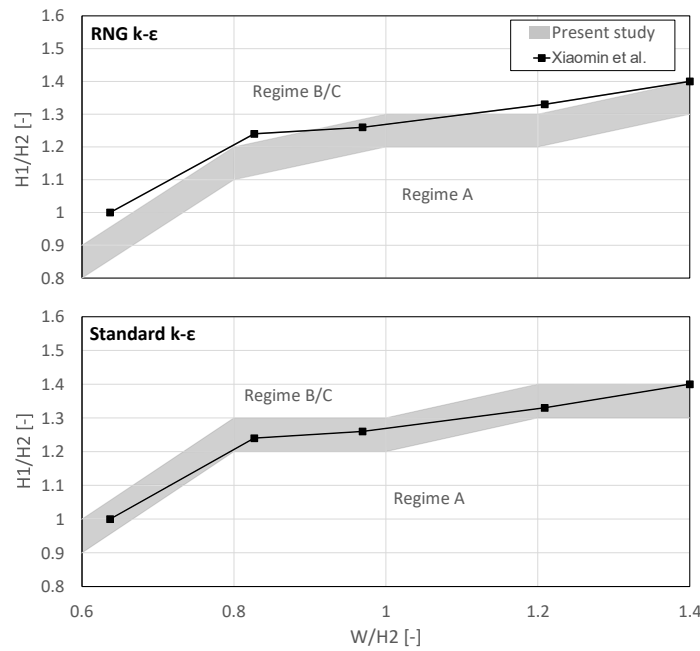


Fig. 7. Comparison of regime changing zones between the present study and the results of Xiaomin et al. (2006) using RNG and standard $k-\epsilon$ turbulent closure.

4.2. Impact of the regimes on pollutant dispersion

Three examples of pollutant dispersion in the street canyon for each regime are shown in Fig. 8. The overall concentrations in the street canyons being very different between the three regimes, the color scale is different for each of them. The velocity vectors are provided in order to better understand the differences in the concentration fields for the three regimes.

The evolution of the concentration field, the overall magnitude of concentration, and the most impacted building are directly linked with the type of regime being established. In regime A, the pollutants released at ground level are mostly dispersed towards the leeward building due to the single clockwise vortex established in the street. In regime B, the apparition of a second vortex due to the increase of the leeward building height and the decrease of the distance between building leads to a change in the dispersion of pollutants. The vortex in the street being in this case counter clockwise, the most impacted building became the windward building. Moreover, concentrations are overall higher in this case and it seems to be the consequence of the clockwise vortex localized just above which is driving a part of the pollutants which left the street to the street again. For the last regime, regime C, both buildings are highly impacted. The difference with the regime B is not only the apparition of a third vortex, but the fact that two vortices are localized in the street between the buildings. Due to this two vortices, the pollutants released at ground level are dispersed to the leeward building but, because of the second vortex in the canyon, they are more homogenized in the low part of the street and seem to be more stagnant. It should also be noted that global velocities in the street tend to decrease with the increase of the leeward building height and the decrease of the distance between building which also conduct to higher pollutant concentrations.

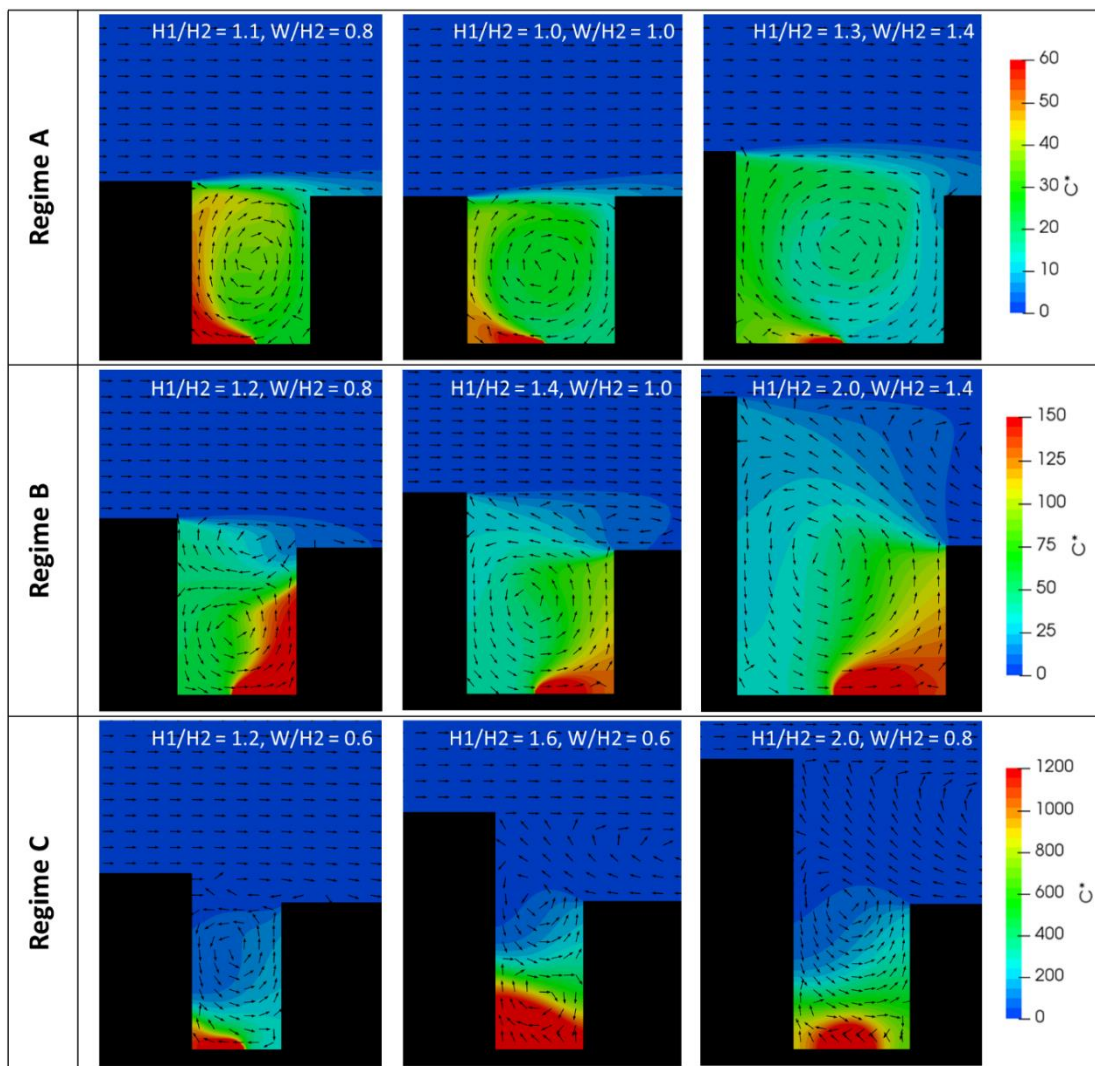


Fig. 8. Three examples of dimensionless concentrations in a street canyon for each type of regime.

4.3. Mean concentration in the street canyon

Initially, the results were studied by considering the mean concentrations of the whole street. Fig. 9 shows the dimensionless street averaged concentrations (i.e. the mean concentration of the $W \times H2$ surface) proposed for several $H1/H2$ and $W/H2$ ratios and the different types of regime are also specified.

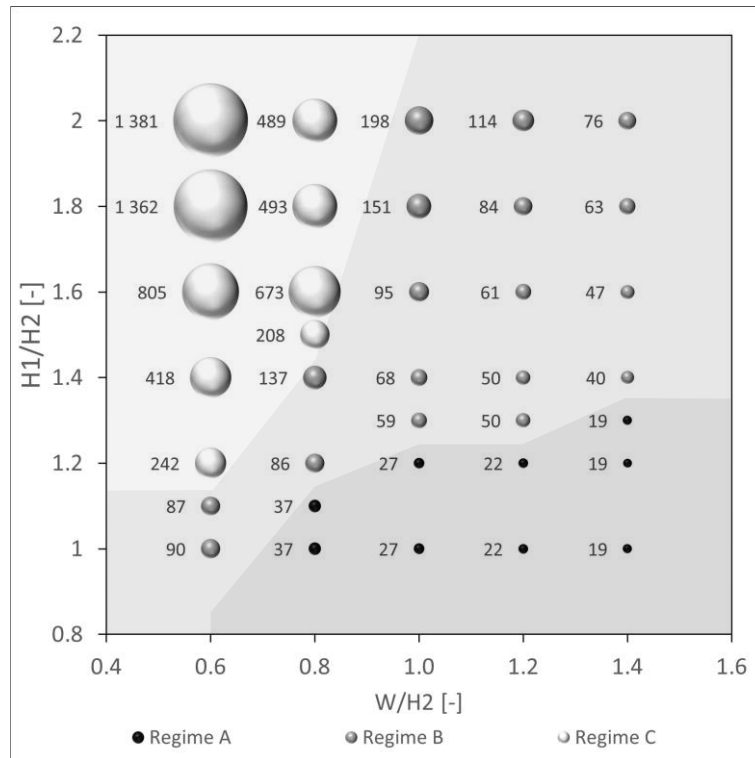


Fig. 9. Dimensionless street averaged concentrations according to the ratio $H1/H2$ and $W/H2$

The results show that the evolution of mean concentrations is highly dependent on the type of regime in place. The mean concentrations are indeed highest when regime C is in place and lowest when regime A is in place.

In regime A, for a given distance between buildings (i.e. a given $W/H2$), the mean concentrations are the same whatever the height of the leeward building. Thus, only the distance between buildings has an impact on the mean concentrations in the street. For a fixed leeward building height, the mean concentrations in the street increase when the distance between buildings decrease. This increase is not constant and becomes higher when ratio $W/H2$ decreases. For example, the mean concentration increases by 23% between $W/H2=1.2$ and $W/H2=1.0$ and then by 37% between $W/H2=1.0$ and $W/H2=0.8$. Lastly, for the $H1/H2$ and $W/H2$ ratios studied in this work, the factor between the lowest and the highest mean concentration for regime A is equal to 2.

In regime B, the evolution of the mean street concentrations is dependent on both ratios $H1/H2$ and $W/H2$: for a given leeward building height, the mean street concentrations increase when the distance between the buildings decreases; for a given distance between buildings, the mean concentration increases when the leeward building height increases. In addition, the increases between mean concentrations are not constant and become higher when $H1/H2$ increases and $W/H2$ decreases. The factor between the highest and lowest mean concentrations in the case of regime B is around 5.

In regime C, the evolution of the street mean concentrations is also dependent on both ratios $H1/H2$ and $W/H2$ but is no longer monotonous. Indeed, for a given distance between the buildings, the mean street concentrations first increase and then become constant. If the leeward building height is high enough, this mean concentration can then decrease. In this third case, a maximal mean concentration is reached. Mean street

concentrations are highest for this regime with, in the worst-case concentrations, 50 times that of the regular case $H1/H2=W/H2=1.0$.

Lastly, considering the whole series of simulations run in this study, for a given $H1/H2$ ratio, the mean concentrations increase as the distance between buildings decreases, whatever the three regimes observed. The evolution of the mean concentrations for a given $W/H2$ is nevertheless dependent on the regime.

4.4. Mean concentration on the building sides

The results were then studied considering only the windward and the leeward building sides. Fig. 10 shows the dimensionless windward side averaged concentrations (i.e. the mean concentrations averaged over the windward profile) proposed for several $H1/H2$, and $W/H2$ ratios and the different types of regime are also specified. Fig. 11 gives the same information, but considering the dimensionless, averaged leeward side concentrations (i.e. the mean concentrations averaged over the leeward profile).

As can be seen in Fig. 10. and Fig. 11., the evolution of the mean concentrations on the two building sides are similar. However, the mean concentrations could be higher or lower on the windward side, depending on the recirculation regimes.

In Regime A, for a given distance between buildings (i.e. a given $W/H2$ ratio), the mean leeward and windward concentrations are constant whatever the $H1/H2$ ratio. However, the mean concentration values are different, with concentrations globally twice as high on the leeward side. This observation is linked to the characteristics of regime A described in section 4.1. Indeed, for all the cases in which regime A occurs, a large clockwise rotating vortex appears which spreads the pollutants released at ground level to the leeward side.

In regime B, the mean concentrations are no longer constant for a given distance between buildings but depend on both ratios $H1/H2$ and $W/H2$. This time the mean concentrations are higher on the windward side according to the counterclockwise vortex occurring in regime B, which spreads the pollutants released at ground level to the windward side. The mean concentrations on the windward side are globally three times higher than those of the leeward side.

In regime C, the mean concentrations still depend on both ratios $H1/H2$ and $W/H2$ and the concentrations are much higher than in regime B. The mean concentrations are globally higher on the leeward side but this is not always true. Indeed, for $H1/H2=2.0$ and $W/H2=0.8$, the mean windward concentration is higher. It is much more difficult to interpret this difference than those of the two previous regimes because two vortices are localized in the canyon in this case. However, in this case the vortex is clockwise and localized near the emission source. The pollutants released near the ground are thus initially spread to the leeward side and it is only afterwards that the second vortex spreads them to the windward side. This explains why the mean concentrations are mostly higher on the leeward side than on the windward side.

Finally, if we focus on how the mean concentrations evolve when the regimes change (e.g. when switching from regime A to regime B), there is a notable difference between the windward and leeward sides. Indeed, for a switch from regime A to regime B, whereas the mean concentrations increase by a factor 6 on the windward side, the concentrations on the leeward side are almost equal. Moreover, on the leeward side, the mean concentration observed in the case of regime B did not increase much when $H1/H2$ increased or $W/H2$ decreased compared to the windward side.

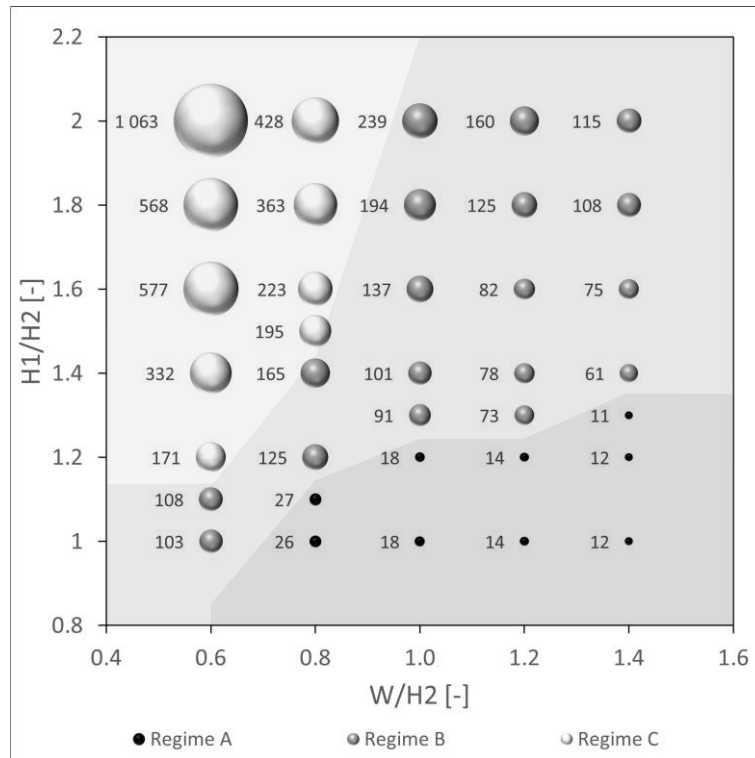


Fig. 10. Dimensionless windward profile averaged concentrations according to the ratios H_1/H_2 and W/H_2 .

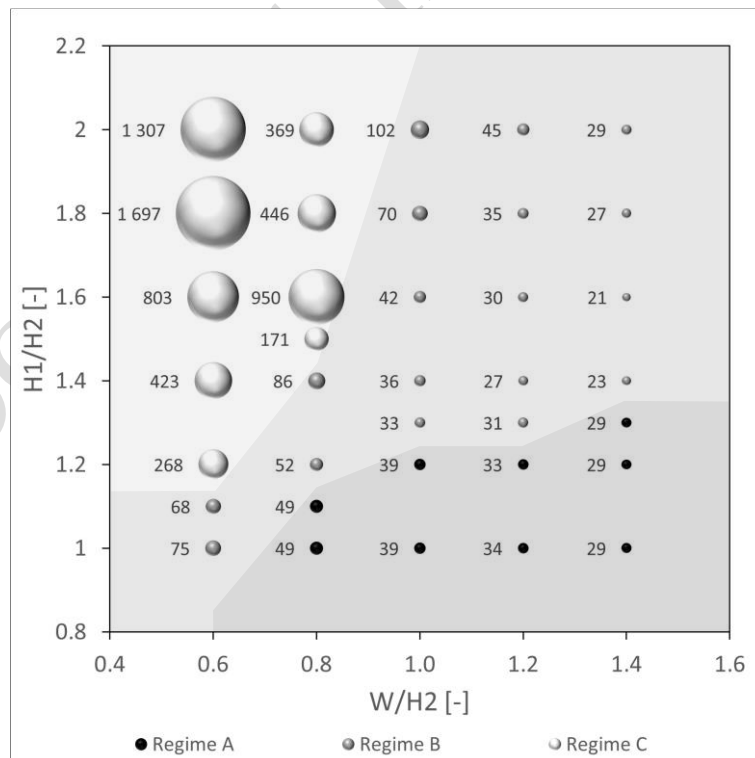


Fig. 11. Dimensionless leeward profile averaged concentrations according to the ratios H_1/H_2 and W/H_2 .

4.5. Mean concentration at ground level

Finally, the results were studied at ground level and Fig. 12 shows the dimensionless ground averaged concentrations (i.e. the mean concentrations averaged over the ground profile) proposed for several $H1/H2$ and $W/H2$ ratios; the different types of regime are also specified.

At ground level, the evolution of mean concentrations is similar for the leeward profile and the whole street: regime A leads to constant mean concentrations for a given distance between buildings; regime B leads to mean concentrations depending on both the distance between buildings and difference in height between the two buildings; regime C leads to the same observation as regime B, the difference being that for a given distance between buildings, a maximal mean concentration is reached, after which this concentration decreases with the increase in the difference in height between the two buildings.

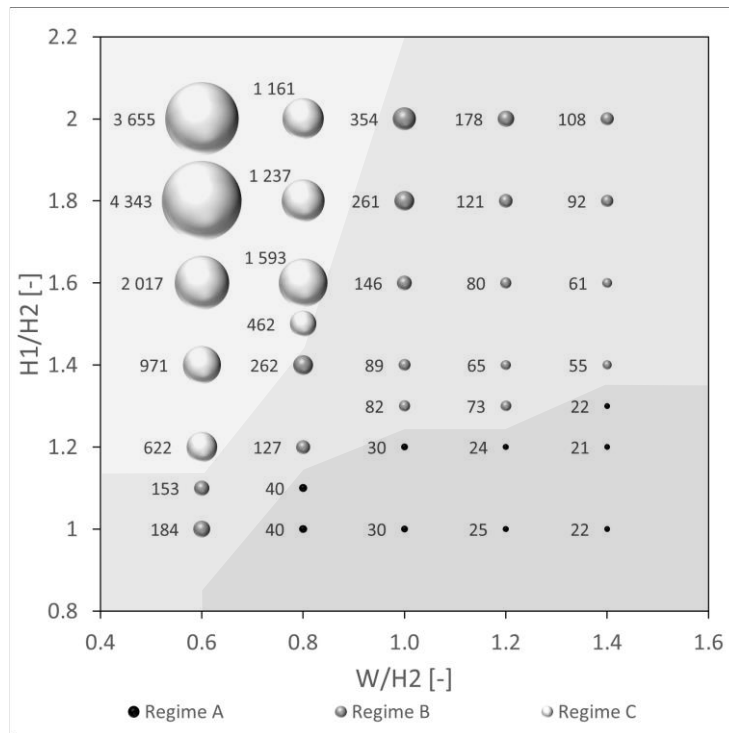


Fig. 12. Dimensionless ground profile averaged concentrations according to ratio $H1/H2$ and $W/H2$.

5. Discussion

Choices were made regarding the turbulence model used as well as the isothermal assumption taken to fulfil this work. These choices could affect the presented results and are worth discussing about.

Based on comparison with experimental data, the RNG turbulence model was selected. This model is an isotropic linear $k-\epsilon$ based model that is known to have some limitations for highly transient cases, especially in a wake of a body, including flows behind the leeward walls of street canyons. To avoid such problems, non-linear turbulence models or anisotropic models such as the Reynolds Stress Model (RSM) should be used. However, these models are time consuming and are more difficult to converge. In addition, they seem to give not as much improvements as expected in the case of

isolated buildings or street canyons. Indeed, Papageorgakis and Assanis (1999) showed that the linear RNG k- ϵ turbulence model gives significant improvements compared to the standard turbulence model for recirculatory flow such for backward facing step cases. Moreover, according to the same authors, the non-linear RNG turbulence model is not very attractive, yielding not to great improvements. Finally, Koutsourakis et al. (2012) showed for six street canyons with different aspect ratios that the RNG turbulence model gives the best performances for each case compared to the standard turbulence model as well as compared to RSM.

The whole study was conducted considering neutral (isothermal) conditions since ambient and wall temperatures were considered equal. Thus, only the forced convection due to the wind was considered. More complex cases could appear when the building walls are heated by solar radiations conducting to unstable conditions where natural convection appears. For this cases, results in terms of recirculation regimes or pollutant concentrations can be different. Wang et al. (2011) studied the cases of leeward, ground, and windward heated walls in a regular street canyon and compared the results with the neutral case (without wall heating). They found that, except for the case of the windward heated wall, the recirculation pattern in the street is always the same. Concentrations are different depending on the case, but they are always lower than for the neutral case. These results are confirmed by Allegrini et al. (2013) who did the same work with several wind speed and also simulated a case where all walls are heated. This case also leads to the same recirculation pattern as for the neutral case. According to these results, it could be said that the results given in this study are not only good for one considering neutral cases but are also a good first approximation of thermally unstable cases. Pollutant concentrations being greater for the neutral case than for the unstable case leading thus to a safer approach.

6. Conclusion

The effects of step-down street canyon geometric properties on recirculation patterns and mean pollutant concentrations in a street were studied with a CFD model. This study considered 6 height ratios $H1/H2$ (from 1.0 to 2.0 with a 0.2 step) and 5 width ratios $W/H2$ (from 0.6 to 1.4 with a 0.2 step). The main conclusions are as follows:

- (a) Three types of regimes can occur as a function of both the height and width ratios of the street. Flow velocities and direction in the street, and thus pollutant concentrations, depend heavily on the type of regime being established. The three types of regime were characterized by the number of vortices established and their direction: regime A corresponded to a single clockwise vortex in the canyon; regime B corresponded to a counter-clockwise vortex in the canyon and a clockwise vortex over the windward building; regime C corresponded to two contra-rotating vortices in the canyon and a clockwise vortex over the windward building.
- (b) The critical values of $H1/H2$ corresponding to a change in the type of regime for a given width ratio were determined. The critical values obtained were differed as a function of the turbulence closure scheme used. These differences were never greater than 0.1 when using standard or RNG k-epsilon turbulence schemes.
- (c) Whatever the mean concentration considered (in the whole canyon, at pedestrian level or near the building faces), the mean concentrations were lowest in the case of regime A and highest in the case of regime C. Regime B therefore corresponded to an intermediary state.
- (d) The mean concentrations increased globally as differences in building height increased ($H1/H2$ ratio), and with the decrease of street width ($W/H2$), except for the case of regime A where the evolutions of mean concentrations depended only on street width.

- (e) The quantitative evolution of the mean pollutant concentration in the whole street at pedestrian level and near the building faces was proposed.

As a summary, in order to have a good ventilation in step-down street canyons and in the perspective of reducing mean pollutant concentration of the whole street at pedestrian level and near building faces, we recommend choosing carefully the height ratio $H1/H2$ as well as the width ratio $W/H2$ in order to be in the case of a regime A.

These conclusions and results were obtained for a given type of street canyon and they should be extended to consider other types such as step-up street canyons and wider and deeper canyons. Moreover, these results were obtained considering flat roofs. However, this type of roof is not the only kind of roof used for buildings and further works should be carried out to obtain information on other types of roof.

Acknowledgments

We would like to thank the ANRT (Association Nationale de la Recherche et de la Technologie) for their support.

References

- Addepalli, B., Pardyjak, E.R., 2015. A study of flow fields in step-down street canyons. *Environmental Fluid Mechanics* 15, 439–481. <https://doi.org/10.1007/s10652-014-9366-z>
- Allegrini, J., Dorer, V., Carmeliet, J., 2013. Wind tunnel measurements of buoyant flows in street canyons. *Building and Environment* 59, 315–326. <https://doi.org/10.1016/j.buildenv.2012.08.029>
- Anderson, J.D., 2009. *Fundamentals of Aerodynamics* 1131.
- Aristodemou, E., Boganegra, L.M., Mottet, L., Pavlidis, D., Constantinou, A., Pain, C., Robins, A., ApSimon, H., 2018. How tall buildings affect turbulent air flows and dispersion of pollution within a neighbourhood. *Environmental Pollution* 233, 782–796. <https://doi.org/10.1016/j.envpol.2017.10.041>
- Bibri, S.E., Krogstie, J., 2017. Smart sustainable cities of the future: An extensive interdisciplinary literature review. *Sustainable Cities and Society* 31, 183–212. <https://doi.org/10.1016/j.scs.2017.02.016>
- Bijad, E., Delavar, M.A., Sedighi, K., 2016. CFD simulation of effects of dimension changes of buildings on pollution dispersion in the built environment. *Alexandria Engineering Journal* 55, 3135–3144. <https://doi.org/10.1016/j.aej.2016.08.024>
- Cui, P.-Y., Li, Z., Tao, W.-Q., 2016. Buoyancy flows and pollutant dispersion through different scale urban areas: CFD simulations and wind-tunnel measurements. *Building and Environment* 104, 76–91. <https://doi.org/10.1016/j.buildenv.2016.04.028>
- Franke, J., Hellsten, A., Schlünzen, H., Carissimo, B., 2007. Best practice guideline for the CFD simulation of flows in the urban environment. COST Action 732.

- Gerdes, F., Olivari, D., 1999. Analysis of pollutant dispersion in an urban street canyon. *Journal of Wind Engineering and Industrial Aerodynamics* 82, 105–124. [https://doi.org/10.1016/S0167-6105\(98\)00216-5](https://doi.org/10.1016/S0167-6105(98)00216-5)
- Hotchkiss, R.S., Harlow, F.H., 1973. Air Pollution Transport in Street Canyons. U.S. Environmental Protection Agency Report (EPA-R4-73-029), pp.129.
- Koutsourakis, N., Bartzis, J.G., Markatos, N.C., 2012. Evaluation of Reynolds stress, $k-\epsilon$ and RNG $k-\epsilon$ turbulence models in street canyon flows using various experimental datasets. *Environmental Fluid Mechanics* 12, 379–403. <https://doi.org/10.1007/s10652-012-9240-9>
- Pavageau, M., Schatzmann, M., 1999. Wind tunnel measurements of concentration fluctuations in an urban street canyon. *Atmospheric Environment* 33, 3961–3971. [https://doi.org/10.1016/S1352-2310\(99\)00138-7](https://doi.org/10.1016/S1352-2310(99)00138-7)
- Qin, Y., Kot, S.C., 1993. Dispersion of vehicular emission in street canyons, Guangzhou City, South China (P.R.C.). *Atmospheric Environment. Part B. Urban Atmosphere* 27, 283–291. [https://doi.org/10.1016/0957-1272\(93\)90023-Y](https://doi.org/10.1016/0957-1272(93)90023-Y)
- Roache, P.J., 1994. Perspective: A Method for Uniform Reporting of Grid Refinement Studies. *Journal of Fluids Engineering* 116, 405. <https://doi.org/10.1115/1.2910291>
- Santiago, J.L., Martin, F., 2005. Modelling the air flow in symmetric and asymmetric street canyons. *International Journal of Environment and Pollution* 25, 145. <https://doi.org/10.1504/IJEP.2005.007662>
- Soulhac, L., Mejean, P., Perkins, R.J., 2001. Modelling the transport and dispersion of pollutants in street canyons. *International Journal of Environment and Pollution* 16, 404. <https://doi.org/10.1504/IJEP.2001.000636>
- Takano, Y., Moonen, P., 2013. On the influence of roof shape on flow and dispersion in an urban street canyon. *Journal of Wind Engineering and Industrial Aerodynamics* 123, 107–120. <https://doi.org/10.1016/j.jweia.2013.10.006>
- Tominaga, Y., Stathopoulos, T., 2017. Steady and unsteady RANS simulations of pollutant dispersion around isolated cubical buildings: Effect of large-scale fluctuations on the concentration field. *Journal of Wind Engineering and Industrial Aerodynamics* 165, 23–33. <https://doi.org/10.1016/j.jweia.2017.02.001>
- Tominaga, Y., Stathopoulos, T., 2007. Turbulent Schmidt numbers for CFD analysis with various types of flowfield. *Atmospheric Environment* 41, 8091–8099. <https://doi.org/10.1016/j.atmosenv.2007.06.054>
- Vardoulakis, S., Fisher, B.E.A., Pericleous, K., Gonzalez-Flesca, N., 2003. Modelling air quality in street canyons: a review. *Atmospheric Environment* 37, 155–182. [https://doi.org/10.1016/S1352-2310\(02\)00857-9](https://doi.org/10.1016/S1352-2310(02)00857-9)
- Vardoulakis, S., Gonzalez-Flesca, N., Fisher, B.E.A., 2002. Assessment of traffic-related air pollution in two street canyons in Paris: implications for exposure studies. *Atmospheric Environment* 36, 1025–1039. [https://doi.org/10.1016/S1352-2310\(01\)00288-6](https://doi.org/10.1016/S1352-2310(01)00288-6)

- Wang, P., Zhao, D., Wang, W., Mu, H., Cai, G., Liao, C., 2011. Thermal Effect on Pollutant Dispersion in an Urban Street Canyon. *International Journal of Environmental Research* 5, 813–820. <https://doi.org/10.22059/ijer.2011.388>
- Wen, H., Malki-Epshtein, L., 2018. A parametric study of the effect of roof height and morphology on air pollution dispersion in street canyons. *Journal of Wind Engineering and Industrial Aerodynamics* 175, 328–341. <https://doi.org/10.1016/j.jweia.2018.02.006>
- Xiaomin, X., Huang, Z., Wang, J., 2006. The impact of urban street layout on local atmospheric environment. *Building and Environment* 41, 1352–1363. <https://doi.org/10.1016/j.buildenv.2005.05.028>
- Yakhot, V., Orszag, S.A., Thangam, S., Gatski, T.B., Speziale, C.G., 1992. Development of turbulence models for shear flows by a double expansion technique. *Physics of Fluids A: Fluid Dynamics* 4, 1510–1520. <https://doi.org/10.1063/1.858424>

Accepted manuscript